**Atmospheric
Chemistry
and Physics
Discussions**

A mechanistic model of global soil nitric oxide emissions: implementation and space based-constraints

R. C. Hudman[1], N. E. Moore[2,*], R. V. Martin[2,3], A. R. Russell[1], A. K. Mebust[1], L. C. Valin[1], and R. C. Cohen[1]

[1]Department of Chemistry, University of California Berkeley, Berkeley, CA, USA
[2]Department of Physics and Atmospheric Science, Dalhousie University, Halifax, Nova Scotia, Canada
[3]Harvard-Smithsonian Center for Astrophysics, Cambridge, MA, USA
*now at: Department of Physics & Astronomy, University of Manitoba, Winnipeg, Manitoba, Canada

Correspondence to: R. C. Cohen (rccohen@berkeley.edu)

ACPD

12, 3555–3594, 2012

A mechanistic model of global soil nitric oxide emissions

R. C. Hudman et al.

Title Page

Abstract	Introduction
Conclusions	References
Tables	Figures

|◄ | ►|
◄ | ►

Back | Close

Full Screen / Esc

Printer-friendly Version

Interactive Discussion

Abstract

Soil emissions have been identified as a major source (∼15 %) of global nitrogen oxide (NO$_x$) emissions. Parameterizations of soil NO$_x$ emissions (S_{NO_x}) for use in the current generation of chemical transport models were designed to capture mean seasonal behaviour. These parameterizations do not, however, respond quantitatively to the meteorological triggers that result in pulsed S_{NO_x} as are widely observed. Here we present a new mechanistic parameterization of S_{NO_x} implemented into a global chemical transport model (GEOS-Chem). The parameterization represents available nitrogen (N) in soils using biome specific emission factors, online wet- and dry-deposition of N as well as fertilizer and manure N derived from a spatially explicit dataset distributed using seasonality derived from data obtained by the Moderate Resolution Imaging Spectrometer. Moreover, it represents the functional form of emissions derived from point measurements and ecosystem scale experiments including pulsing following soil wetting by rain or irrigation, and emissions that are a smooth function of soil moisture. This parameterization yields global above-soil S_{NO_x} of 10.7 Tg N yr^{-1}, including 1.8 Tg N yr^{-1} from fertilizer N input (0.68 % of applied N) and 0.5 Tg N yr^{-1} from atmospheric N deposition. Over the United States Great Plains, S_{NO_x} are predicted to comprise 15–40 % of the tropospheric NO$_2$ column and increase column variability by a factor of 2–4 during the summer months due to chemical fertilizer application and warm temperatures. S_{NO_x} enhancements of 50–80 % of the simulated NO$_2$ column are predicted over the African Sahel during the monsoon onset (April–June). In this region the day-to-day variability of column NO$_2$ is increased by a factor of 5 due to pulsed-N emissions. We evaluate the model by comparison to observations of the NO$_2$ column from the OMI instrument. We find the model is able to reproduce observations of pulsed-N induced interannual variability over the US Great Plains. We also show that the OMI mean (median) NO$_2$ on the overpass following first rainfall over the Sahel is 49 % (23 %) higher than in the five days preceding. The measured NO$_2$ on the day after rainfall is still 23 % (5 %) higher, providing a direct measure of the pulse's decay time of 1–2 days. This is consistent

Full Screen / Esc

Printer-friendly Version

Interactive Discussion

with the pulsing representation used in our parameterization and much shorter than 5–14 day pulse decay length used in current models.

1 Introduction

Nitric oxide emissions from microbial processes in soils represent ∼15 % of the modern global atmospheric NO_x source (∼50 % in preindustrial times) and are a major contribution to the NO_x budget outside of cities (Holland et al., 1999). Atmospheric NO_x is thus coupled to the Earth's nitrogen cycle through a complex web of interactions involving soil microbial activity, soil nitrogen (N) content and anthropogenic fertilizer rates. Understanding and modeling these interactions is essential to predicting atmospheric composition and to understanding the direct and indirect effects of atmospheric NO_x on ozone, aerosol, and climate.

While the outline of the biogeochemistry of NO_x emissions has been well established, identifying details of the mechanisms and strategies for scaling from laboratory and point measurements in the field to ecosystem scales or to the larger scales of regional and global models remains challenging and both poorly evaluated and verified. Measurements using soil chambers in the field and laboratory experiments show that soil NO_x emissions (S_{NO_x}) vary greatly with climate and edaphic conditions, but are most strongly correlated with N-availability, temperature and soil moisture, making S_{NO_x} dependent on regional temperature and precipitation patterns and fertilizer management practices (e.g., Williams and Fehsenfeld, 1991; Bouwman et al., 2002; Meixner and Yang, 2006; Hudman et al., 2010). However, the advent of space-based measurement capabilities for column NO_2 measurement provides a new opportunity to observe S_{NO_x} over larger domains and to capture statistics of their variability in space and time as the emissions respond to meteorological drivers and to anthropogenic fertilizer.

Here, we present an updated global S_{NO_x} parameterization, the Berkeley-Dalhousie Soil NO_x Parameterization (BDSNP), which includes a more physical representation

of the key processes derived from field measurements than did previous parameterizations: (1) soil moisture and temperature dependence are decoupled allowing for a continuum of S_{NO_x} response rather than discrete wet or dry states, and (2) pulsing length and strength is modified to depend on soil moisture history rather than precipitation amounts. Additionally, we update fertilizer-maps and treatments of S_{NO_x}: (a) N fertilizer emissions are updated using latest gridded inventories for chemical fertilizers and manure, (b) seasonality derived from data obtained by the Moderate Resolution Imaging Spectrometer (MODIS) is used to account for timing and distribution of N fertilizer, (c) N fertilizer is now incorporated into a parameter representing the standing pool of N in the soils and otherwise treated identically to the natural pool of N, responding to temperature and soil moisture and resulting in pulsed emissions, and (d) wet and dry deposition of ammonia (NH_3), ammonium (NH_4^+), nitric acid (HNO_3), nitrate (NO_3^-), nitrogen dioxide (NO_2), and peroxyacetyl nitrate (PAN) are included as terms affecting the soil N pool and thus affect S_{NO_x}. After describing this new parameterization and its implementation in the GEOS-Chem chemical transport model (CTM), we describe comparison of the predictions to those made with recent implementations of a model by Yienger and Levy (1995) (YL95) and some initial attempts at evaluation of the BDSNP using satellite observations.

2 Prior parameterizations

S_{NO_x} have been estimated on regional and global scales using process-based models (Potter et al., 1996; Parton et al., 2001), empirical models (Yienger and Levy, 1995; Yan et al., 2005; Delon et al., 2007; Steinkamp and Lawrence, 2011), and by scaling field observations (Davidson and Kingerlee, 1997) with global above-canopy estimates ranging from 4.7–13 Tg N yr^{-1} (Table 1). Most process-based gaseous N models use an implementation of the conceptual hole-in-the pipe model of Firestone and Davidson (1989), where N-emission (N_2O, NO, N_2) is proportional to nitrification/denitrification rates, soil gas diffusivity and other edaphic conditions (Potter et al.,

A mechanistic model of global soil nitric oxide emissions

R. C. Hudman et al.

1996; Parton et al., 2001; Butterbach-Bahl et al., 2009). For example, the NASA-CASA model (Potter et al., 1996) assumes that a fixed 2 % of mineralized N is emitted as some form of $NO:N_2O:N_2$ depending on soil moisture availability. To account for the pulsing of dry soils, the DAYCENT model (Parton et al., 2001) uses a parameterization based on
5 precipitation history (Yienger and Levy, 1995), while the CASA and the DNDC model (Butterbach-Bahl et al., 2009) do not account for pulsed emissions. Pulsed emissions have been shown to contribute regionally up to 22 % of annual emissions (Davidson et al., 1992) and satellite observations (including those described below) suggest the fraction might be larger in many locations (e.g., Bertram et al., 2005; Hudman et al.,
10 2010).

YL95 and its recent implementations

At present, S_{NO_x} processes are represented in most CTMs using various implementations of the empirical scheme developed by Yienger and Levy (1995) (YL95), which computes emissions as a function of temperature, precipitation, fertilizer application,
15 vegetation type, and canopy-cover (e.g., Bey et al., 2001; Emmons et al., 2010). Regional comparisons with surface and satellite observations, however, suggest the standard YL95 scheme results in emissions that are a factor of 2–4 too low (e.g., Wang et al., 2007; Boersma et al., 2008; Zhao et al., 2009; Steinkamp and Lawrence, 2011; Lin, 2011). In principle, it is possible to create a set of regionally corrected parameters,
20 as Bertram et al. (2005) did for a single emission episode in the northern Great Plains of the United States. Current CTMs, however, carry much more information about the water cycle than was available at the time YL95 was developed allowing a model that includes additional mechanistic details.

The current implementation of the YL95 scheme in GEOS-Chem, as described in
25 Wang et al. (1998), produces above-soil estimates of 7.4 Tg N yr^{-1} for the year 2006 (Fig. 1a). S_{NO_x} are computed as a function of vegetation type (Olson, 1992), temperature, precipitation history, and fertilizer use:

$$S_{NO_x} \text{ Flux} = f_{w/d}\left(T, A_{w/d,\text{biome}}\right) \times P(\text{precipitation}) + E_{\text{Fert}}, \tag{1}$$

where $f_{w/d}$ is a constant, linear, or exponential function of soil temperature (T) and $A_{w/d,\text{biome}}$ is a coefficient to distinguish between vegetation type. Soils are labeled as either wet ("w") or dry ("d") with separate temperature dependencies for each, leading

5 to sharp steps in emissions that are independent of soil moisture. This functional relationship is depicted in Fig. 2. $P(\text{precipitation})$ is a scaling factor used to adjust the flux during pulsing events, which is a function of precipitation amount over dry soils. The model treats natural emissions and fertilizer emissions differently. E_{Fert} represents fertilizer emissions, which in prior versions of GEOS-Chem is set to 2.5 %

10 of total fertilizer applied, evenly emitted over the growing season and these emissions do not respond to meteorological variables with the same functional form as natural N emissions. A time series of simulated fertilizer emissions over the central United States (103.75–93.75° W, 27–51° N) is shown in Fig. 3. In GEOS-Chem a scaling factor is added to account for loss of NO_x to plant canopy based on Jacob and Bakwin (1991).

15 Recent observations regarding the canopy reduction factor, however, provide mixed evidence and laboratory measurements of NO_2 compensation points suggest that NO_2 should be emitted from forest canopies at low NO_x concentrations (Raivonen et al., 2009; Chaparro-Suarez et., 2011). Given this uncertainty, we do not consider canopy reduction and focus on above-soil estimates here.

20 Figure 1a shows yearly averaged S_{NO_x} from the original implementation of the YL95 scheme in GEOS-Chem. The largest emissions are predicted over Northern Hemisphere agricultural regions (India, northeastern China, and the central United States) and over northern equatorial Africa. Disagreement exists between this estimate and top-down estimates, which indicate that YL95 underestimates emissions by

25 factors of 2–3 in several regions including the United States, Mexico, Eastern China, and northern equatorial African grasslands (Jaeglé et al., 2005; Wang et al., 2007; Boersma et al., 2008). Globally, space-based observations of NO_2 columns from the Global Ozone Monitoring Experiment (GOME, 40 × 320 km nadir footprint, with global coverage ~weekly) were used to derive a yearly global S_{NO_x} a posteriori source of

Title Page

Abstract	Introduction
Conclusions	References
Tables	Figures

|◄ | ►|

◄ | ►

Back | Close

Full Screen / Esc

Printer-friendly Version

Interactive Discussion

$8.9\,\mathrm{Tg\,N\,yr^{-1}}$, 68 % greater than YL95 $S_{\mathrm{NO_x}}$ estimates (Jaeglé et al., 2005). These studies suggest a discrepancy in the functional relationships with soil-moisture and in the representation of N fertilizer.

There have been several empirical models of $S_{\mathrm{NO_x}}$ introduced since YL95. Similar to YL95, Yan et al. (2005) derive an exponential relationship between $S_{\mathrm{NO_x}}$ and temperature, but added additional coefficients in the exponent to account for soil organic carbon, pH, and land cover type. Additionally, they updated the pulsing scheme to include stronger, shorter pulses based on dry-spell length rather than precipitation amount, consistent with more recent studies. Steinkamp and Lawrence (2011) recalculate the wet and dry biome coefficients ($A_{\mathrm{w/d,biome}}$) used in YL95 with an updated database of 560 measurements. The above studies describe discrete wet and dry states, rather than a continuous dependence on soil moisture. A regional non-linear regression model was created using observations over Europe relating $S_{\mathrm{NO_x}}$ to seven climatic and soil condition variables (Delon et al., 2007). Delon et al. (2008) updated this model for use over Africa and found a continuous dependence on soil moisture was crucial to correctly represent temporal variability in $S_{\mathrm{NO_x}}$.

3 Soil NO$_x$ parameterization

The BDSNP represents $S_{\mathrm{NO_x}}$ in a functional form consistent with measurements and biological and meteorological drivers:

$$S_{\mathrm{NO_x}}\ \mathrm{Flux} = A'_{\mathrm{biome}}(N_{\mathrm{avail}}) \times f(T) \times g(\theta) \times P(l_{\mathrm{dry}}). \tag{2}$$

Fertilizer N, the standing pool of N and deposited N are represented in the term N_{avail}. A'_{biome} coefficients are functions of N_{avail} and the $A_{\mathrm{w,biome}}$ coefficients from YL95, updated to latest literature estimates from Steinkamp and Lawrence (2011). The temperature and soil moisture dependencies $f(T)$ and $g(\theta)$, where θ is water-filled pore space, are represented as continuous functions. Pulsing P depends on dry spell length l_{dry} resulting in stronger, shorter pulses based on the parameterization of Yan et al. (2005).

These individual terms are described in detail below. A central tool in the analysis is the GEOS-Chem model which is described in Appendix A.

3.1 Soil moisture/soil temperature dependence

The temperature dependence of S_{NO_x} in the BDSNP combines an exponential dependence on temperature between 0 °C and 30 °C (constant at $T > 30$) and a Poisson function scaling for soil moisture:

$$f(T) \times g(\theta) = e^{0.103T} \times a\theta e^{-b\theta^2}. \tag{3}$$

The parameterization for soil moisture effects takes advantage of new meteorological fields available in the GEOS-5 assimilated meteorological product. Water-filled pore space, θ, is defined as the ratio of the volumetric soil moisture content to the porosity (Linn and Doran, 1984). Dividing by porosity acts as a normalizing step that makes θ satisfy $0 \leq \theta \leq 1$, allowing comparison between soils of different textures (Otter et al., 1999). In the GEOS-Chem meteorological fields, θ is available for the top 2 cm of soil, where the majority of S_{NO_x} originate (Pierce and Aneja, 2000).

The response of S_{NO_x} is not monotonic to θ. S_{NO_x} are low for the extreme values of θ (0 and 1). For low values, emissions are water-limited. For high values, denitrification dominates preferentially emitting N_2O and N_2. S_{NO_x} dependence on soil moisture is thus best described as a Poisson function (Parsons et al., 1996; Otter et al., 1999; Pierce and Aneja, 2000; Kirkman et al., 2001; van Dijk and Meixner, 2001; van Dijk et al., 2002) where the values of a and b are chosen such that the maximum value (unity) occurs for $\theta = 0.2$ for arid soils and 0.3 elsewhere. Laboratory and field measurements have found that emissions peak in this range for most soils (Yang and Meixner, 1997; Ormeci et al., 1999).

Figure 2 shows the BDSNP soil moisture/temperature dependence for grasslands compared with YL95. YL95 label soil as either "dry" or "wet" based on the prior two week precipitation and have separate soil temperature dependencies for each. A wet soil is one that has received in excess of 10 mm of rainfall in the previous two weeks,

Full Screen / Esc

Printer-friendly Version

Interactive Discussion

otherwise, it is dry. For wet soils, emissions are described by a linearly increasing function (with zero intercept) for temperatures between 0 and 10 °C and an exponentially increasing function for temperatures between 10 °C and 30 °C. For dry soils, emissions are described by a linearly increasing function for temperatures between 0 and 30 °C. The BDSNP avoids these sharp steps, and is instead a smooth function of soil moisture and temperature consistent with field and laboratory studies.

3.2 Pulsing

Pulsed S_{NO_x} occur when very dry soil is wetted resulting in a reactivation of water-stressed bacteria. Here, we follow the parameterization by Yan et al. (2005) derived from four field studies, which relate pulsed emissions to antecedent dry period (Johansson et al., 1988; Davidson et al. 1991; Scholes et al., 1997; Martin et al., 1998):

$$P(l_{dry}, t) = \left[13.01 \ln\left(l_{dry}\right) - 53.6\right] \times e^{-ct} \tag{4}$$

P represents the magnitude of the peak flux relative to the pre-wetting flux, and the constant c is a rate constant representing the rise/fall time of the pulse ($c = 0.068\,h^{-1}$). The value of l_{dry} is the antecedent dry period in hours. The two main differences between this treatment and that used by YL95 are that P_{peak} depends logarithmically on the antecedent dry period and the condition for a pulse is a change in soil moisture rather than rainfall. We use the two-part condition described in Yan et al. (2005) to check for pulsing potential. The dry period is defined as time since volumetric soil moisture content decreased to less than 17.5 % (v/v). A pulse occurs when there is a soil moisture increase of 0.5 % (v/v). Assuming soil bulk density of 1.4 Mg m^{-3} (typical of seasonally dry savannahs), this is equivalent to $\theta \sim 0.3$ and a $\Delta\,\theta > 0.01$, which we use here.

3.3 Soil N content

We use a spatially explicit chemical fertilizer (70 Tg N yr^{-1}) and manure (128 Tg N yr^{-1}) dataset from Potter et al. (2010) with a native resolution of 0.5 × 0.5°, valid for the year

2000 (available at http://www.geog.mcgill.ca/~nramankutty/Datasets/Datasets.html). We assume 37 % of manure N, 47 Tg N yr^{-1}, remains or is applied as N input (Sheldrick et al., 2003). To introduce timing, the satellite instruments MODIS and TRMM (Tropical Rainfall Measuring Mission) are used to give information regarding the start and end of the growing season of each model grid square. Zhang et al. (2006) describe an algorithm for deriving growing season start and end dates using a time series of MODIS enhanced vegetation index (EVI). We use growing season dates derived from the MODIS Land Cover Dynamics product (MCD12Q2) averaged over 2001 to 2004 and regridded to the GEOS-Chem model to define the beginning and end of the growing season respectively (Fig. 4) (Ganguly et al., 2010). We apply 75 % of the yearly fertilization amount over the first month as a Gaussian distribution around the green-up day and the remaining 25 % is applied evenly over the remaining time in the growing season. This 75/25 treatment is the most typical global farming practice (Matson et al., 1998).

To determine the dynamic N fertilizer available in the soil, we solve the mass-balance equation:

$$N_{avail}(t) = N_{avail}(0)e^{-t/\tau} + F \times \tau \times (1 - e^{-t/\tau}), \tag{5}$$

where N_{avail} is the mass of available nitrogen in the soil (ng N m^{-2}), F is the application rate, and τ is a decay lifetime. Based on measurements within the top 10 cm of soil, the decay constant (τ) for fertilizer N is chosen as 4 months, with values in the literature for agricultural soils ranging from 2 months to 7 months (Matson et al., 1998; Chen et al., 2004; Russell et al., 2006). The value of F varies over the growing season as described above. At the end of the growing season (Fig. 4), the value of F is zero and the remaining N fertilizer in the soil is left to decay.

We include wet and dry deposition of N species as an additional fertilizer source. Online wet and dry deposition rates of NH_3, NH_4, HNO_3, NO_3^-, NO_2, and PAN are archived each dynamic time step in GEOS-Chem (Liu et al., 2001). Other N-species add minimal amounts to N-deposition and are neglected. We assume 60 % of this

deposited N enters the soil, with continental values in literature ranging from 55 % to 80 % (Gleick, 1993). The remainder is lost to runoff into waterways. Available N in soil is then calculated as with fertilizer (Eq. 5). The decay constant (τ) for deposition is chosen to be 6 months based on measurements made over lands with natural vegetation, with measurements ranging from 4 months to 1 yr (Hart et al., 1993; Nadelhoffer et al., 1995).

3.4 Biome emission factors

The biome emission factor is a crude measure of the N available in soils. We choose emission factors A'_{biome} (ng N m^{-2} s^{-1}) to be functions of the wet biome-dependent emission factors $A_{\text{w,biome}}$ from Steinkamp and Lawrence (2011), which were derived from 560 measurements for 23 land types, and available nitrogen from fertilizer and deposited N emissions, N_{avail}:

$$A'_{\text{biome}} = A_{\text{w,biome}} + N_{\text{avail}} \times \overline{E}. \tag{6}$$

Instead of choosing an emission rate for each box equivalent to 2.5 % of applied N yearly as done in the YL95 scheme, we choose the mean emission rate, $\overline{E}$, so that the total global above-soil NO$_x$ emissions due to fertilizer matches observed estimates of fertilizer emissions of 1.8 Tg N yr^{-1} (0.5 % of N-fertilizer applied) from Stehfest and Bouwman (2006), which in GEOS-Chem is 0.68 % of available N. Figure 3 shows fertilizer-induced S_{NO_x} averaged over the central Great Plains (27–51° N, 101.25–91.25° W) for 2006 compared with the original scheme implemented into GEOS-Chem. Fertilizer is now treated identically to the natural pool of N responding to temperature/soil moisture and results in pulsed emissions, rather than a constant flux over the growing season.

4 Results for the year 2006

The new model produces above-soil S_{NO_x} of $10.7\,Tg\,N\,yr^{-1}$ compared to the original model of $7.4\,Tg\,N\,yr^{-1}$. Figure 1 shows the annual mean S_{NO_x} for the original YL95 model as implemented in GEOS-Chem and the new BDSNP presented here for 2006.

5   The largest S_{NO_x} increases are predicted over fertilized fields in northern midlatitudes, over seasonally dry grasslands of Africa and South America, and over forested regions in central Africa. Decreases are predicted over South American tropical forests and over inundated soils of India and Indonesia during the wet season, all of which were previously held constant and are now allowed to respond to temperature and soil

10   moisture changes.

The implementation of the soil temperature/soil moisture (Sect. 3.1) treatment decreases S_{NO_x}. The wet coefficients $A_{w,biome}$ of the original YL95 model are much greater ($\sim \times 7$) than the dry coefficients $A_{d,biome}$ meaning that emissions remained high throughout the rainy season and low throughout the dry season. The BDSNP rep-

15   resents the onset and eventual inundation of tropical/sub-tropical monsoons, increasing S_{NO_x} during the dry season, relative to the low value forced in the YL95 parameterization, and decreasing emissions over tropical forests now subject to temperature/moisture fluctuations.

The new pulsing scheme increases S_{NO_x} over seasonally wet grasslands/savannahs.

20   The largest increases are seen over the African Sahel during the onset of the wet season. First rains reactivate bacteria water-stressed from the long dry season, releasing NO as a byproduct (Davidson et al., 1992). As the excess N is consumed, NO emissions remain high compared to the dry season (Serca et al., 1998). A similar response is seen over the savannahs/grasslands of South America and Australia. Compared to

25   the original GEOS-Chem implementation of YL95 which used climatological precipitation to determine the "wet" and "dry" criteria of soils and thus exhibited no interannual variability, the new parameterization has a meteorologically driven timing of the onset of the dry and wet season, as well as allowing for drying out of soils. These changes

improve the comparison with observations of both magnitude and timing of pulsed N events. For example, June 2006 was anomalously dry and warm over the US Great Plains leading to a 50 % increase in emissions (Hudman et al., 2010).

The new fertilizer treatment contributes $+1.8\,\mathrm{Tg\,N\,yr^{-1}}$ S_{NO_x} compared to the original fertilizer implementation which contributed $0.8\,\mathrm{Tg\,N\,yr^{-1}}$. Addition of deposited N to the pool of available N contributes an additional $0.5\,\mathrm{Tg\,N\,yr^{-1}}$ to the emissions.

5 Model evaluation

A detailed validation of regionally and globally applied S_{NO_x} models with available surface observations is not possible. Field measurements are often set up to test functional relationships in idealized settings, rather than the regional-scale response, and are of varying duration, making scaling highly uncertain and dependent on available measurements. Steinkamp and Lawrence (2011) recalculated the $A_{w/d,biome}$ coefficients used in YL95 with an updated database of 560 measurements. Using the geometric mean of $A_{w/d,biome}$ values calculated over each land type they find a global above-soil total of $10.5\,\mathrm{Tg\,N\,yr^{-1}}$. Using the arithmetic mean of $A_{w/d,biome}$ values calculated, however, they find a global above-soil total of $33\,\mathrm{Tg\,N\,yr^{-1}}$, illustrating the large variability in the measurements. We use the geometric mean here as it is most consistent with the upper range expected; global values of above-soil S_{NO_x} from previous modeling efforts and scaling from field-observations range from 6.6–$22\,\mathrm{Tg\,N\,yr^{-1}}$ (Table 1).

To date, revised inventories based on satellite measurements effectively assume a grid cell specific adjustment to source strength which is not understood at the process scale. Satellite observations of NO_2 have advanced such that they can now provide daily global coverage at fine spatial resolution. The Ozone Monitoring Instrument (OMI, $13 \times 24\,\mathrm{km}$ nadir footprint, overpass time ~13:45 LT, with global coverage ~daily), launched aboard the Aura satellite in fall 2004, has high spatio-temporal resolution

compared with previous instruments, allowing for stronger constraints on not only the magnitude, but on regional-scale responses governing S_{NO_x} variability (Hudman et al., 2010). Here, we use tropospheric NO_2 vertical column densities from the Ozone Monitoring Instrument (OMI) to provide initial attempts at constraining the regional-scale response of S_{NO_x} to soil moisture, temperature, and fertilization.

5.1 Sensitivity of OMI NO_2 columns to S_{NO_x}

To identify regions where validation is possible, we use GEOS-Chem to determine the locations and time-periods in which S_{NO_x} are expected to dominate the tropospheric NO_2 column over non-soil sources of NO_x (i.e., anthropogenic, biomass burning and lightning emissions). The largest S_{NO_x} are expected during the Northern Hemisphere late spring (April–June) due to pulsed emissions over seasonally dry soils and summer (June–August) due to chemical fertilizer application and warm temperatures. We include above-soil S_{NO_x} without canopy reduction.

Figure 5a–b shows the GEOS-Chem simulated seasonal mean ratio of soil to total columns, where the soil column is defined as the difference between a simulation with and without S_{NO_x}. During the onset of the summer monsoon over the northern equatorial tropics, soil columns are predicted to comprise between 0–65 % of the total column, with large S_{NO_x} enhancements over the African Sahel (15–65 %, boxed region Fig. 5a). The contribution of S_{NO_x} over fertilized midlatitudes ranges from 0–60 % (Fig. 5b) and is large during the summer months over the Great Plains of the United States (0–50 %, boxed region Fig. 5b).

S_{NO_x} are variable day-to-day, reflecting synoptic variability in temperatures and pulsing associated with wetting and drying of soils. Figure 5c–d shows the ratio of the standard deviation in the soil columns to the standard deviation in the total columns without S_{NO_x}. This measure can be used to diagnose the contribution of S_{NO_x} to observed column variability. Over the African Sahel the soil column variability is 5× greater than the variability in the absence of S_{NO_x}, suggesting daily soil pulsing should be easily visible over other sources of variability. Over most of the industrialized midlatitudes this ratio

is ~1 indicating S_{NO_x} are not important to the variability in the NO_2 column. The Great Plains are an exception and the variability due to S_{NO_x} is increased (×2–4). Using this metric as a guide, we focus our validation on these two regions.

5.2 Validation of fertilizer source: interannual variability over the Great Plains

Hudman et al. (2010) examined the interannual variability in the NO_2 column over North America measured by OMI in 2005–2008. They found that much of the observed variability in June was due to meteorological variability interacting with the large volume of fertilizer applied to the region. Dry, warm conditions in June 2006 followed by convective precipitation induced pulsed emissions of NO_x over the agricultural Great Plains with a different timing than in the years 2005, 2007 and 2008. Using OMI tropospheric NO_2 column measurements regridded to $0.25 \times 0.25°$ resolution and a model of S_{NO_x}, they inferred a 50 % increase in S_{NO_x} and up to a 30 % increase in the tropospheric NO_2 column in 2006 relative to the June 2005–2008 mean.

Figure 6 shows the tropospheric NO_2 column deviations from the June 2005–2008 mean from OMI, and simulated by GEOS-Chem using the BDSNP over the central United States. All column data are regridded daily to $2 \times 2.5°$ resolution where cloud radiance fraction <50 % and then averaged to produce the monthly mean columns. Several retrievals exist for calculating NO_2 column densities from the earthshine radiance observed by OMI. All products begin with the same NO_2 slant column densities; determined using a non-linear least squares fit of the ratio of measured radiance to solar irradiance spectra in the 405–465 nm window. Differences in the resulting tropospheric NO_2 vertical column densities arise from differences in the methodology used to calculate the stratospheric component of the slant column and the tropospheric air mass factor, which converts the slant column to vertical column density. Here we compare two retrievals as a measure of uncertainty in the NO_2 anomaly (retrievals are described in Appendix B): the GEOS-Chem DOMINO Product (DP_GC) (Lamsal et al., 2010), adapted from the DOMINO product (Boersma et al., 2007), and the BErkeley High-Resolution product (BEHR) (Russell et al., 2011). The June 2006 mean

Title Page

Abstract | Introduction

Conclusions | References

Tables | Figures

|◄ | ►|

◄ | ►

Back | Close

Full Screen / Esc

Printer-friendly Version

Interactive Discussion

(total) anomaly over the central Great Plains (27–51° N, 101.25–91.25° W, boxed region Fig. 5b, d) is +11 % (2.5 Gg N) from the DP_GC retrieval and +11 % (3.9 Gg N) from the BEHR retrieval. We compare these values to a GEOS-Chem simulation without lightning NO_x emissions as flash rates in the model are scaled monthly by grid box to match climatology (Murray et al., 2012), impacting interannual variability. In GEOS-Chem using the BDSNP the mean anomaly of +8 % (2.1 Gg N) is in good agreement with satellite observations, giving us confidence in the soil moisture/temperature relationship used as well as the magnitude of the fertilizer response.

5.3 Validation of pulsing scheme: monsoonal onset over the African Sahel

Observations show large pulses of S_{NO_x} when dry grasslands/savannahs or seasonally dry forests are exposed to rainfall (Johansson and Sanhueza, 1988; Davidson, 1992; Harris et al., 1996; Levine et al., 1996; Kirkman et al., 2001; Scholes et al., 1997; Serca et al., 1998; Stewart et al., 2008). To test our parameterization of these pulsing events, we focus on the central Sahel (0–30° W, 12–18° N), a region of transition between the Sudanian savannahs in the south and Sahara desert in the north during spring 2006 (Fig. 7a). The dry season in this region extends from October to June, during which S_{NO_x} effectively shut off due to lack of moisture, and N accumulates in the soil (Sect. 2.1). The first rains of the wet season reactivate water-stressed bacteria releasing large pulses of gaseous NO (Davidson, 1992; Jaeglé et al., 2004). First rains arrive in the southern Sahel in May, with first rains moving further north by early June (Fig. 7b).

In the Yan et al. (2005) parameterization used here, rainfall following a two month dry period results in a ×40 increase in S_{NO_x}, decaying to ×8 in 24 h and to ×1.5 after 48 h. To test the length of the pulse duration we examine the OMI NO_2 columns from the Standard Product (SP, Level 2, Version 1.0.5, Collection 3) before and following first rains of the 2006 wet season. This analysis was performed with SP, as BEHR is only available over the continental United States and the DP_GC data used was provided at lower resolution than 0.25 × 0.25°; however, use of a different retrieval is not

predicted to produce significantly different results. Figure 8 shows mean and median enhancements in NO_2 column over central Sahelian grasslands following first rainfall. Ratios are taken against the average NO_2 column in the 5 days preceding first rainfall. All column data are averaged daily to $0.25 \times 0.25°$ resolution where cloud radiance fraction <50 %. Mean (Median) columns are 49 % (23 %) higher than in the five days preceding the first rainfall. The following day, columns are still 23 % (5 %) higher but any relationship breaks down in the subsequent days, suggesting pulses last on average 1–2 days, consistent with the representation in the BDSNP. For comparison to the GEOS-Chem simulation at $2 \times 2.5°$ resolution, we change the dry spell criteria to 0.025 mm, to account for the coarser resolution. The model predicts the first day of rain NO_2 columns to be 46 % (28 %) higher. The following day pulse is 34 % (21 %) higher. As in the OMI observations the pulse decays to background within 1–2 days.

6 Conclusions

We present the BDSNP, a global model of S_{NO_x} that builds on the YL95 parameterization currently used in most atmospheric chemical transport and air quality models. The BDSNP is designed to represent the mechanisms that govern the spatial and temporal patterns of S_{NO_x} with the spatiotemporal resolution of the underlying meteorological model. The BDSNP includes a dependence on soil moisture, representation of biogeochemistry that induces pulsing of the emissions following dry spells, and a detailed spatial and temporal representation of N-inputs both from chemical/manure fertilizer and atmospheric N-deposition. The original YL95 scheme as implemented into GEOS-Chem for 2006 yields global S_{NO_x} estimates of $7.4 \, \text{Tg N yr}^{-1}$ with $0.8 \, \text{Tg N yr}^{-1}$ from chemical fertilizers compared to this implementation of the BDSNP in GEOS-CHEM of $10.7 \, \text{Tg N yr}^{-1}$, with $1.8 \, \text{Tg N yr}^{-1}$ from fertilizer/manure N input (0.68 % of applied N) and $0.5 \, \text{Tg N yr}^{-1}$ from atmospheric N-deposition.

In an initial evaluation of the processes in the BDSNP, we use GEOS-Chem to locate time periods and regions where S_{NO_x} are a large fraction of the tropospheric NO_2

column allowing comparison of model predictions to OMI observations that can be interpreted as primarily due to S_{NO_x}. The largest pulsed enhancements in the model are predicted over the African Sahel during the monsoon onset (April–June), comprising 15–65 % of the simulated NO_2 column and increasing variability by a factor of 5. Over this region the OMI mean (median) NO_2 on the overpass following first rainfall are 49 % (23 %) higher than in the five days preceding. The NO_2 on the day after rainfall is still 23 % (5 %) higher. The BDSNP has similar temporal behaviour in response to rainfall in the Sahel. In the northern midlatitudes, the variability in the NO_2 column due to pulsed S_{NO_x} is smaller than the variability due to synoptic transport of anthropogenic emissions except over the United States Great Plains, where S_{NO_x} are predicted to contribute as much as 60 % of the column and to increase variability by a factor of 2–4. Over the Great Plains, we find the model is able to reproduce the observed interannual variability over the region giving us confidence in the soil moisture/temperature relationship used as well as the magnitude of the fertilizer response.

S_{NO_x} are approximately 15 % of the global N emissions and a dominant source of atmospheric N and its variability in many continental regions. The BDSNP attempts to produce a physically realistic response of S_{NO_x} to meteorological and agricultural drivers thus providing a new opportunity to study the effects of S_{NO_x} on the atmospheric chemistry of O_3, aerosol, and OH. Further, the potential for linkages to N_2O emissions through the soil moisture response might one day be explored. Additional studies are needed to assess the accuracy of this parameterization – especially as applied on regional scales and to pulsing associated with individual meteorological events. Such efforts would be able to evaluate the spatiotemporal patterns with more specificity than we have been able to in this initial evaluation of the model.

Appendix A

GEOS-Chem model

We simulate the impacts of soil NO_x emissions on tropospheric chemistry using the GEOS-Chem global three-dimensional model of tropospheric chemistry (version 8.03, www.geos-chem.org) driven by assimilated meteorological observations from the NASA Goddard Earth Observing System (GEOS-5). Meteorological fields have a temporal resolution of 6 h (3 h for surface variables and mixing depths) with a native horizontal resolution of $0.5 \times 0.667°$, degraded to $2 \times 2.5°$ for input into this simulation using GEOS-Chem. The model is applied to a global simulation of O_3-NO_x-VOC chemistry including a fully coupled aerosol mechanism (Bey et al., 2001; Park et al., 2004). The simulations are conducted for 2005–2008 and are initialized on 1 January 2005 with GEOS-Chem fields generated by a 12-month spin-up simulation at $2 \times 2.5°$ resolution from chemical climatology.

Global anthropogenic emissions are from EDGAR 3.2FT2000 inventory (Olivier et al., 2001) for the year 2000 (van Donkelaar et al., 2008). These are overwritten regionally with the US Environmental Protection Agency National Emission Inventory for 1999 (EPA-NEI99) NEI 99 with modifications described by Hudman et al. (2007, 2008), including a generalized 50 % decrease in NO_x emissions from power plants and industry reflecting 1999–2004 reductions (Frost et al., 2006). Mexican emissions are from Big Bend Regional Aerosol and Visibility Observational (BRAVO) Study Emissions Inventory for 1999 (Kuhns et al., 2005). Canadian emissions are based on the CAC inventory (http://www.ec.gc.ca/pdb/cac/) for 2005. East Asian emissions are for the year 2006 with monthly variation based on Zhang et al. (2007). European emissions are from the European Monitoring and Evaluation Programme (EMEP) for 2005. Biomass burning emissions are from the interannual Global Fire Emissions Database version 2 (GFED2) inventory with monthly resolution (van der Werf et al., 2006; Randerson et al., 2007).

Soil NO$_x$ emissions (S_{NO_x}) are from the BDSNP presented here and the Yienger and Levy (1995) model as implemented in Wang et al. (1998). Lightning NO$_x$ flash rates are linked to deep convection following the parameterization of Price and Rind (1992) based on GEOS-5 computed cloud-top heights. Flash rates are scaled based for each grid box on monthly average rates from the Lightning Imaging Sensor and Optical Transient Detector satellite instruments (OTD/LIS) (Sauvage et al., 2007; Murray et al., 2012). NO$_x$ yield per flash is 125 mol in the tropics and 500 mol at northern mid-latitudes (north of 30° N) (Hudman et al., 2007) with vertical NO$_x$ emission profiles from Ott et al. (2010).

For comparison with OMI observations, the model NO$_2$ column is sampled daily between 12:00–03:00 p.m. LT corresponding to approximately the OMI overpass time.

Appendix B

Tropospheric NO$_2$ columns from the Ozone Monitoring Instrument

The Ozone Monitoring Instrument is a nadir-viewing UV/Visible spectrometer aboard the EOS-AURA satellite launched in July 2004 into a sun-synchronous orbit with a 13:38 local equator crossing time (Boersma et al., 2002). Earthshine radiance and solar irradiance are recorded at 0.5 nm resolution in the 270–500 nm window which can be used to derive NO$_2$ slant column densities using the DOAS method (Levelt et al., 2006). The 114° field of view is distributed over 60 discrete viewing angles on an imaging array detector perpendicular to the flight direction yielding a 2600 km ground swath, allowing for daily global coverage. Pixel sizes range from 13 × 24 km to 40 × 128 km at the edge of the sampling swath.

We use three independent retrievals of tropospheric NO$_2$ column data from OMI observations described briefly below: the Standard Product (SP) Level 2, Version 1.0.5, Collection 3 available from the NASA Goddard Earth Sciences Data and Information Services Center DISC (http://daac.gsfc.nasa.gov/Aura/OMI/omno2.shtml) described in

Bucsela et al. (2006) and Celarier et al. (2008), the GEOS-Chem DOMINO Product (DP_GC) described in Lamsal et al. (2010), and the Berkeley High Resolution Retrieval (BEHR) described in Russell et al. (2011). The three products begin with the same NO_2 slant column densities. Differences in the resulting tropospheric NO_2 vertical column densities arise from the methods used to calculate the stratospheric component of the slant column and the tropospheric air mass factor, which converts the slant column to vertical column density. For all retrievals we exclude pixels with cloud radiance fractions greater than 50 %.

B1   Standard product

The stratospheric contribution to the total column is calculated by masking regions where tropospheric NO_2 columns are high ($>0.5 \times 10^{15}$) and applying a wave-2 smoothing in the meridional direction on remaining pixels. The tropospheric AMF is computed using a look-up table based on surface albedo, terrain pressure, viewing parameters and NO_2 profile shape. Surface albedo is from a monthly $1 \times 1°$ database from Koelemeijer et al. (2003). Terrain pressure is from the SDP Toolkit 90 arsec DEM map. NO_2 profiles are from a $2 \times 2.5°$ gridded dataset of annual mean profiles from the GEOS-Chem model.

B2   DP_GC

The DP_GC product is based on the DOMINO algorithm retrieval (Level 2, Version 1.0.2, Collection 3) described in detail in Boersma et al. (2007). In the DOMINO algorithm, the stratospheric slant column is derived by assimilating OMI NO_2 slant columns into the TM4 global chemical transport model run at $3 \times 2°$. Surface albedo is from a monthly $1 \times 1°$ database from Koelemeijer et al. (2003). NO_2 vertical profiles and terrain pressure are interpolated from the TM4 model output. The DP_GC replaces these NO_2 profiles with GEOS-Chem run at $2 \times 2.5°$ and adds a cross-track bias correction.

B3 BEHR

The BErkeley High Resolution Retrieval (BEHR) uses the stratospheric removal method of the Standard Product above. Tropospheric AMFs are similarly calculated using a look-up table, but with higher spatial and temporal resolution inputs. Surface albedo is from $0.05 \times 0.05°$ MODIS MCD43C3, provided as a 16 day average every 8 days. Terrain pressure is from GLOBE 1km x 1km tropographical database averaged to OMI pixel. NO_2 profiles are from a 4×4 km monthly WRF-Chem simulation (averaged to OMI pixel).

B4 Error

The total error in the tropospheric NO_2 column retrieved is 0.75×10^{15} molec. cm^{-2} for the slant column density, 0.15×10^{15} molec. cm^{-2} and 0.2×10^{15} molec. cm^{-2} for the stratospheric subtraction for the SP and DOMINO product respectively. Tropospheric AMF errors arise from input parameters of albedo, terrain pressure, and NO_2 profile shape, as well as aerosol assumptions and cloud properties. AMF induced NO_2 column errors are estimated at ~30 % for clear sky and ~60 % for cloudy conditions (Boersma et al., 2004).

References

Bertram, T. H., Heckel, A., Richter, A., Burrows, J. P., and Cohen, R. C.: Satellite measurements of daily variations in soil NO_x emissions, Geophys. Res. Lett., 32, L24812, doi:10.1029/2005GL024640, 2005.

Bey, I., Jacob, D. J., Yantosca, R. M., Logan, J. A., Field, B. D., Fiore, A. M. Li, Q., Liu, H. Y., Mickley, L. J., and Schultz, M. G.: Global modeling of tropospheric chemistry with assimilated meteorology: Model description and evaluation, J. Geophys. Res., 106, 23073–23095, 2001.

Boersma, K. F., Bucsela, E. J., Brinksma, E. J., and Gleason, J. F: NO_2, in: OMI Algorithm Theoretical Basis Document, Vol. 4, OMI Trace Gas Algorithms, ATBD-OMI-04 (Version 2), 13–36, 2002.

Boersma, K. F., Eskes, H. J., and Brinksma, E. J.: Error analysis for tropospheric NO_2 retrieval from space, J. Geophys. Res., 109, D04311, doi:10.1029/2003JD003962, 2004.

Boersma, K. F., Eskes, H. J., Veefkind, J. P., Brinksma, E. J., van der A, R. J., Sneep, M., van den Oord, G. H. J., Levelt, P. F., Stammes, P., Gleason, J. F., and Bucsela, E. J.: Near-real time retrieval of tropospheric NO_2 from OMI, Atmos. Chem. Phys., 7, 2103–2118, doi:10.5194/acp-7-2103-2007, 2007.

Boersma, K. F., Jacob, D. J. , Bucsela, E.J.,. Perring, A. E, Dirksen, R. , van der A, R. J., Yantosca, R. M., Park, R. J., Wenig, M. O., Bertram, T. H. and Cohen, R. C.: Validation of OMI tropospheric NO_2 observations during INTEX-B and application to constrain NO_x emissions over the eastern United States and Mexico, Atmos. Environ., 42, 4480–4497, 2008.

Bouwman, A. F., L. J. M. Boumans, and Batjes, N. H.: Emissions of N_2O and NO from fertilized fields: Summary of available measurement data, Global Biogeochem. Cy., 16, 1058, doi:10.1029/2001GB001811, 2002.

Bucsela, E. J., Celarier, E. A., Wenig, M. O., Gleason, J. F., Veefkind, J. P., Boersma, K. F., and Brinksma, E. J.: Algorithm for NO_2 vertical column retrieval from the Ozone Monitoring Instrument, IEEE T. Geosci. Remote, 44, 1245–1258, 2006.

Butterbach-Bahl, K., M. Kahl, L. Mykhayliv, C. Werner, R. Kiese, and Li, C.: A European-wide inventory of soil NO emissions using the biogeochemical models DNDC/Forest-DNDC, Atmos. Environ., 43, 1392–1402, 2009.

Celarier, E. A., Brinksma, E. J., Gleason, J. F., Veefkind, J. P., Cede, A., Herman, J. R., Ionov, D., Goutail, F., Pommereau, J. –P., Lambert, J. –C., van Roozendael, M., Pinardi, G., Wit-

trock, F., Schönhardt, A., Richter, A., Ibrahim, O. W., Wagner, T., Bojkov, B., Mount, G., Spinei, E., Chen, C. M., Pongetti, T. J., Sander, S. P., Bucsela, E. J., Wenig, M. O., Swart, D. P. J., Volten, H., Kroon, M., and Levelt, P. F.: Validation of Ozone Monitoring Instrument nitrogen dioxide columns, J. Geophys. Res., 113, D15S15, doi:10.1029/2007JD008908, 2008.

Chaparro-Suarez, I. G., Meixner, F. X., and Kesselmeier, J.: Nitrogen dioxide (NO_2) uptake by vegetation controlled by atmospheric concentrations and plant stomatal aperture, Atmos. Environ., 45, 5742–5750, 2011.

Chen, X., Zhang, F., Römheld, V., Horlacher, D., Schulz, R., Böning-Zilkens, M., Wang, P., and Claupein, W.: N_2O and NO production in various Chinese agricultural soils by nitrification, Soil Biol. Biochem., 36, 953–963, 2004.

Davidson, E. A.: Pulses of nitric oxide and nitrous oxide flux following the wetting of dry soil: An assessment of probable sources and importance relative to annual fluxes, Ecol. Bull., 42, 149–155, 1992b.

Davidson, E. A. and Kingerlee, W.: A global inventory of nitric oxide emissions from soils, Nutr. Cycl. Agroecosyst., 48, 37–50, 1997.

Delon C., Serca, D., Boissard, C., Dupont, R., Dutot, A., Laville, P., de Rosnay, P., and Delmas, R.: Soil NO emissions modeling using artificial neural network, Tellus B, 59B, 502–513, 2007.

Delon, C., Reeves, C. E., Stewart, D. J., Serça, D., Dupont, R., Mari, C., Chaboureau, J.-P., and Tulet, P.: Biogenic nitrogen oxide emissions from soils – impact on NO_x and ozone over West Africa during AMMA (African Monsoon Multidisciplinary Experiment): modelling study, Atmos. Chem. Phys., 8, 2351–2363, doi:10.5194/acp-8-2351-2008, 2008.

Emmons, L. K., Walters, S., Hess, P. G., Lamarque, J.-F., Pfister, G. G., Fillmore, D., Granier, C., Guenther, A., Kinnison, D., Laepple, T., Orlando, J., Tie, X., Tyndall, G., Wiedinmyer, C., Baughcum, S. L., and Kloster, S.: Description and evaluation of the Model for Ozone and Related chemical Tracers, version 4 (MOZART-4), Geosci. Model Dev., 3, 43–67, doi:10.5194/gmd-3-43-2010, 2010.

Firestone, M. K. and Davidson, E. A.: Microbiological basis of NO and N_2O production and consumption in soil. In: Andreae, M. O. and Schimel, D. S. (Eds.), Exchange of trace gases between terrestrial ecosystems and the atmosphere, Wiley, Chichester, 7–21, 1989.

Frost, G. J., McKeen, S. A., Trainer, M., Ryerson, T. B., Neuman, J. A., Roberts, J. M., Swanson, A., Holloway, J. S., Sueper, D. T., Fortin, T., Parrish, D. D., Fehsenfeld, F. C., Flocke, F., Peckham, S. E., Grell, G. A., Kowal, D., Cartwright, J., Auerbach, N., and Habermann, T.:

A mechanistic model of global soil nitric oxide emissions

R. C. Hudman et al.

Title Page

Abstract	Introduction
Conclusions	References
Tables	Figures

|◄ | ►|

◄ | ►

Back | Close

Full Screen / Esc

Printer-friendly Version

Interactive Discussion

Effects of changing power plant NO_x emissions on ozone in the eastern United States: Proof of concept, J. Geophys. Res., 111, D12306, doi:10.1029/2005JD006354, 2006.

Galbally, I. E. and Roy, C. R.: Loss of fixed nitrogen from soils by nitric oxide exhalation, Nature, 275, 734–735, 1978.

Ganguly, S., Friedl, M. A., Tan, B., Zhang, X., and Verma, M.: Land surface phenology from MODIS: Characterization of the Collection 5 global land cover dynamics product, Remote Sens. Environ., 114, 1805–1816, 2010.

Gleick, P. H.: Water in Crisis, Oxford University Press, New York, 1993.

Harris, G. W., Wienhold, F. G., and Zenker, T.: Airborne observations of strong biogenic NO_x emissions from the Namibian Savanna at the end of the dry season, J. Geophys. Res.-Atmos., 101, 23707–23711, 1996.

Hart, S. C., Firestone, M. K., Paul, E. A., and Smith, J. L.: Flow and fate of soil nitrogen in an annual grassland and a young mixed-conifer forest, Soil Biol. Biochem., 25, 431–442, 1993.

Holland, E. A., Dentener, F. J., and Braswell, B. H.: Contemporary and pre-industrial global re-active nitrogen budgets, Biogeochemistry, 46, 7–43, doi:10.1023/A:1006148011944, 1999.

Hudman, R. C., Jacob, D. J., Turquety, S., Leibensperger, E. M., Murray, L. T., Wu, S., Gilliland, A. B., Avery, M., Bertram, T. H., Brune, W., Cohen, R. C., Dibb, J. E., Flocke, F. M., Fried, A., Holloway, J., Neuman, J. A., Orville, R., Perring, A., Ren, X., Sachse, G. W., Singh, H. B., Swanson, A., and Wooldridge, P. J.: Surface and lightning sources of nitrogen oxides over the United States: Magnitudes, chemical evolution, and outflow, J. Geophys. Res., 112, D12S05, doi:10.1029/2006JD007912, 2007.

Hudman, R. C., Murray, L. T., Jacob, D. J., Millet, D. B., Turquety, S., Wu, S., Blake, D. R., Goldstein, A. H., Holloway, J., and Sachse, G. W.: Biogenic vs. anthropogenic sources of CO over the United States, Geophys. Res. Lett., 35, L04801, doi:10.1029/2007GL032393, 2008.

Hudman, R. C., Russell, A. R., Valin, L. C., and Cohen, R. C.: Interannual variability in soil nitric oxide emissions over the United States as viewed from space, Atmos. Chem. Phys., 10, 9943–9952, doi:10.5194/acp-10-9943-2010, 2010.

Jacob, D. J. and Bakwin, P. S.: Cycling of NO_x in tropical forest canopies and its implications for the global source of biogenic NO_x to the atmosphere, American Society of Microbiology, Washington DC, 1991.

Jaegle, L., Steinberger, L., Martin, R. V., and Chance, K.: Global partitioning of NO_x sources using satellite observations: Relative roles of fossil fuel combustion, biomass burning and

soil emissions, Faraday Discuss., 130, 407–423, 2005.

Johansson, C. and Sanhueza, E.: Emission of NO from savanna soils during the rainy season, J. Geophys. Res., 93, 14193–14198, 1988.

Kirkman, G. A., Yang, W. X., and Meixner, F. X.: Biogenic nitric oxide emissions upscaling: An approach for Zimbabwe, Global Biogeochem. Cy., 15, 1005–1020, 2001.

Koelemeijer, R. B. A., de Haan, J. F., and Stammes, P.: A database of spectral surface reflectivity in the range 335–772 nm derived from 5.5 years of GOME observations, J. Geophys. Res., 108, 4070, doi:10.1029/2002JD002429, 2003.

Kuhns, H., Knipping, E. M., and Vukovich, J. M.: Development of a United States-Mexico emissions inventory for the Big Bend Regional Aerosol and Visibility Observational (BRAVO) Study, JAPCA J. Air Waste M., 55, 677–692, 2005.

Lamsal, L. N., Martin, R. V., van Donkelaar, A., Celarier, E. A., Bucsela, E. J., Boersma, K. F., Dirksen, R., Luo, C., and Wang, Y.: Indirect validation of tropospheric nitrogen dioxide retrieved from the OMI satellite instrument: Insight into the seasonal variation of nitrogen oxides at northern midlatitudes, J. Geophys. Res., 115, D05302, doi:10.1029/2009JD013351, 2010.

Levelt, P. F., Gijsbertus, H. J., van den Oord, H. J., Dobber, M. R., Mälkki, A., Visser, H., de Vries, J., Stammes, P., Lundell, J. O. V., and Saari, H.: The Ozone Monitoring Instrument, IEEE Trans. Geosci. Remote, 44, 5, 1093–1101, 2006.

Levine, J. S., Winstead, E. L., Parsons, D. A. B., Scholes, M. C., Scholes, R. J., Cofer III, W. R., Cahoon Jr., D. R., and Sebacher, D. I.: Biogenic soil emissions of nitric oxide (NO)and nitrous oxide (N_2O) from savannas in South Africa: The impact of wetting and burning, J. Geophys. Res., 101, 23689–23697, 1996.

Lin, J.-T.: Satellite constraint for emissions of nitrogen oxides from anthropogenic, lightning and soil sources over East China on a high-resolution grid, Atmos. Chem. Phys. Discuss., 11, 29807–29843, doi:10.5194/acpd-11-29807-2011, 2011.

Linn, D. M. and Doran, J. W.: Effect of water-filled pore space on carbon dioxide and nitrous oxide production in tilled and nontilled soils, Soil Sci. Soc. Am. J., 48, 1267–1272, 1984.

Liu, H., Jacob, D. J., Bey, I., and Yantosca, R. M.: Constraints from 210Pb and 7Be on wet deposition and transport in a global three-dimensional chemical tracer model driven by assimilated meteorological fields, J. Geophys. Res., 106, 12109–12128, 2001.

Matson, P. A., Naylor, R. L., and Ortiz-Monasterio, I., Integration of environmental, agronomic, and economic aspects of fertilizer management, Science, 280, 112–115, 1998.

A mechanistic model of global soil nitric oxide emissions

R. C. Hudman et al.

Title Page

Abstract	Introduction
Conclusions	References
Tables	Figures

◄ | ►◄

◄ | ►

Back | Close

Full Screen / Esc

Printer-friendly Version

Interactive Discussion

Meixner, F. X. and Yang, W. X.: Biogenic emissions of nitric oxide and nitrous oxide from arid and semi-arid land, in: Dryland Ecohydrology, edited by: D'Odorico, P. and Porporato, A., 233–255, Dordrecht, Berlin Heidelberg New York, ISBN: 1-4020-4261-2, 2006.

Muller, J.-F.: Geographical Distribution and Seasonal Variation of Surface Emissions and Deposition Velocities of Atmospheric Trace Gases, J. Geophys. Res., 97, D43787, doi:10.1029/91JD02757, 1992.

Murray, L. T., Jacob, D. J., Logan, J. A., and Hudman, R. C.: Optimized regional scaling of the lightning source of nitrogen oxides in a global chemical transport model using satellite lightning data: 1. Constraining spatial, seasonal and interannual variability in the lightning flash rate, to be submitted to J. Geophys. Res., 2012.

Nadelhoffer, K. J., Downs, M., Fry, B. Aber, J. D., Magill, A. H., and Melillo, J. M.: The fate of 15N-labeled nitrate additions to a northern hardwood forest in eastern Maine, USA, Oecologia, 103, 292–301, 1995.

Olivier, J. G. J., Berdowski, J. J. M., Peters, J. A. H. W., Bakker, J., Visschedijk, A. J. H., and Bloos, J. P. J.: Applications of EDGAR, including a description of EDGAR 3.2: Reference database with trend data for 1970–1995, Tech. Rep., RIVM Bilthovan, RIVM report, 773301001/ NRP report 4, 2001.

Olson, J.: World Ecosystems (WEI.4): Digital raster data on a 10 minute geographic 1080 × 2160 grid, in: Global ecosystems database, version 1.0: Disc A, edited by: NOAA Natl. Geophys. Data Center, Boulder, Colorado, 1992.

Ormeci, B., Sanin, S. L., and Pierce, J. J.: Laboratory study of NO flux from agricultural soil: Effects of soil moisture, pH, and temperature, J. Geophys. Res., 104, 1621–1629, 1999.

Ott, L. E., Pickering, K. E., Stenchikov, G. L, Allen, D. J., DeCaria, A. J., Ridley, B., Lin, R.-F., Lang, S., and Tao, W.-K.: Production of lightning NO_x and its vertical distribution calculated from three-dimensional cloud-scale chemical transport model simulations, J. Geophys. Res., 115, D04301, doi:10.1029/2009JD011880, 2010.

Otter, L. B., Yang, W. X., Scholes, M. C., and Meixner, F. X.: Nitric oxide emissions from a southern African savanna, J. Geophys. Res., 105, 20697–20706, 1999.

Park, R. J., Jacob, D. J., Field, B. D., Yantosca, R. M., and Chin, M.: Natural and transboundary pollution influences on sulfate-nitrate-ammonium aerosols in the United States: Implications for policy, J. Geophys. Res., 109, D15204, doi:10.1029/2003JD004473, 2004.

Parsons, D. A., Scholes, M. C., Scholes, R. J., and Levine, J. S.: Biogenic NO emissions from savanna soils as a function of fire regime, soil type, soil nitrogen, and water status, J.

A mechanistic model of global soil nitric oxide emissions

R. C. Hudman et al.

Geophys. Res., 101, 23683–23688, 1996.

Parton, W. J., Holland, E. A., Del Grosso, S. J., Hartman, M. D., Martin, R. E., Mosier, A. R., Ojima, D. S., and Schimel, D. S.: Generalized model for NO_x and N_2O emissions from soils, J. Geophys. Res.-Atmos., 106, 17403–17419, 2001.

5   Pierce, J. J. and Aneja, V. P.: Nitric oxide emissions from engineered soil systems, Journal of Environmental Engineering, 225–232, 2000.

Potter, C. S., Matson, P. A., Vitousek, P. M., and Davidson, E. A.: Process modeling of controls on nitrogen trace gas emissions from soils worldwide, J. Geophys. Res., 101, 1361–1377, 1996.

10   Potter, P., Ramankutty, N., Bennet, E. M., and Donner, S. D.: Characterizing the spatial patterns of global fertilizer application and manure production, Earth Interact., 14, 1–22, 2010.

Price, C. and Rind, D.: A simple lightning parameterization for calculating global lightning distributions, J. Geophys. Res., 97, 9919–9933, doi:10.1029/92JD00719, 1992.

Raivonen, M., Vesala, T., Pirjola, L., Altimir, N., Keronen, P., Kulmala, M., and Hari, P.: Compen-

15   sation point of NO_x exchange: Net result of NO_x consumption and production, Agr. Forest Meteorol., 149, 1073–1081, 2009.

Randerson, J. T., van der Werf, G. R., Giglio, L., Collatz, G. J., and Kasibhatla, P. S.: Global Fire Emissions Database, Version 2 (GFEDv2.1), Data set, from Oak Ridge National Laboratory Distributed Active Archive Center, Oak Ridge, Tennessee, USA,

20   doi:10.3334/ORNLDAAC/849, 2007.

Russell, A. R., Perring, A. E., Valin, L. C., Bucsela, E. J., Browne, E. C., Wooldridge, P. J., and Cohen, R. C.: A high spatial resolution retrieval of NO_2 column densities from OMI: method and evaluation, Atmos. Chem. Phys., 11, 8543–8554, doi:10.5194/acp-11-8543-2011, 2011.

Russell, C. A., Dunn, B. W., Batten, G. D., Williams, R. L., and Angus, J. F.: Soil tests to predict

25   optimum fertilizer nitrogen rate for rice, Field Crops Research, 97, 286–301, 2006.

Sauvage, B., Martin, R. V., van Donkelaar, A., Liu, X., Chance, K., Jaeglé, L., Palmer, P. I., Wu, S., and Fu, T.-M.: Remote sensed and in situ constraints on processes affecting tropical tropospheric ozone, Atmos. Chem. Phys., 7, 815–838, doi:10.5194/acp-7-815-2007, 2007.

Scholes, M. C., Martin, R., Scholes, R. J., Parsons, D., and Winstead, E.: NO and N_2O emis-

30   sions from savanna soils following the first simulated rains of the season, Nutr. Cycl. Agroecosyst., 48, 115–122, 1997.

Serça, D., Delmas, R., Le Roux, X., Parsons, D. A. B., Scholes, M. C., Abbadie, L., Lensi, R., Ronce, O., and Labrouc, L.: Comparison of nitrogen monoxide emissions from several

A mechanistic model of global soil nitric oxide emissions

R. C. Hudman et al.

Title Page

Abstract | Introduction

Conclusions | References

Tables | Figures

◄ | ►

◄ | ►

Back | Close

Full Screen / Esc

Printer-friendly Version

Interactive Discussion

African tropical ecosystems and influence of season and fire, Global Biogeochem. Cy., 12, 637–651, 1998.

Sheldrick, W., Syers, J. K., and Lingard, J.: Contribution of livestock excreta to nutrient balances, Nutr. Cycl. Agroecosyst., 66, 119–131, 2003.

5 Stehfest, E. and Bouwman, L.: N_2O and NO emission from agricultural fields and soils under natural vegetation: summarizing available measurement data and modeling of global annual emissions, Nutr. Cycl. Agroecosyst., 74, 207–228, doi:10.1007/s10705-006-9000-7, 2006.

Steinkamp, J. and Lawrence, M. G.: Improvement and evaluation of simulated global biogenic soil NO emissions in an AC-GCM, Atmos. Chem. Phys., 11, 6063–6082, doi:10.5194/acp-
10 11-6063-2011, 2011.

Stewart, D. J., Taylor, C. M., Reeves, C. E., and McQuaid, J. B.: Biogenic nitrogen oxide emissions from soils: impact on NO_x and ozone over west Africa during AMMA (African Monsoon Multidisciplinary Analysis): observational study, Atmos. Chem. Phys., 8, 2285–2297, doi:10.5194/acp-8-2285-2008, 2008.

15 van der Werf, G. R., Randerson, J. T., Giglio, L., Collatz, G. J., Kasibhatla, P. S., and Arellano Jr., A. F.: Interannual variability in global biomass burning emissions from 1997 to 2004, Atmos. Chem. Phys., 6, 3423–3441, doi:10.5194/acp-6-3423-2006, 2006.

van Dijk, S. M. and Meixner, F. X.: Production and consumption of NO in forest and pasture soils from the Amazon basin, Water Air Soil Poll., 1, 119–130, 2001.

20 van Dijk, S. M., Gut, A. , Kirkman, G. A., Meixner, F. X., Andreae, M. O., and Gomes, B. M.: Biogenic NO emissions from forest and pasture soils: Relating laboratory studies to field measurements, J. Geophys. Res., 107, 8058, doi:10.1029/2001JD000358, 2002.

van Donkelaar, A., Martin, R. V., Leaitch, W. R., Macdonald, A. M., Walker, T. W., Streets, D. G., Zhang, Q., Dunlea, E. J., Jimenez, J. L., Dibb, J. E., Huey, L. G., Weber, R., and
25 Andreae, M. O.: Analysis of aircraft and satellite measurements from the Intercontinental Chemical Transport Experiment (INTEX-B) to quantify long-range transport of East Asian sulfur to Canada, Atmos. Chem. Phys., 8, 2999–3014, doi:10.5194/acp-8-2999-2008, 2008.

Wang, Y., Jacob, D. J., and Logan, J. A.: Global simulation of tropospheric O_3-NO_x-hydrocarbon chemistry: 1. Model formulation, J. Geophys. Res., 103, 10713–10725, 1998.

30 Wang, Y. X., McElroy, M. B., Martin, R. V., Streets, D. G., Zhang, Q., and Fu, T.-M.: Seasonal variability of NO_x emissions over east China constrained by satellite observations: Implications for combustion and microbial sources, J. Geophys. Res., 112, D06301, doi:10.1029/2006JD007538, 2007.

Title Page

Abstract | Introduction

Conclusions | References

Tables | Figures

◄◄ | ►►

◄ | ►

Back | Close

Full Screen / Esc

Printer-friendly Version

Interactive Discussion

Williams, E. J. and Fehsenfeld, F. C.: Measurement of nitrogen oxide emissions at three North American ecosystems, J. Geophys. Res., 96, 1033–1042, 1991.

Williams, E. J., Parrish, D. D., and Fehsenfeld, F. C.: Determination of Nitrogen Oxide Emissions From Soils: Results From a Grassland Site in Colorado, United States, J. Geophys. Res., 92, 2173–2179, 1987.

Yan, X., Ohara, T., and Akimoto, H.: Statistical modeling of global soil NO_x emissions, Global Biogeochem. Cy., 19, GB3019, doi:10.1029/2004GB002276, 2005.

Yang, W. X. and Meixner, F. X.: Gaseous nitrogen emissions from grasslands, CAB Int., Wallingford, UK, 67–71, 1997.

Yienger, J. J. and Levy II, H.: Empirical model of global soil-biogenic NO_x emissions, J. Geophys. Res., 100, 11447–11464, 1995.

Zhang, Q., Streets, D. G., He, K., Wang, Y., Richter, A., Burrows, J. P., Uno, I., Jang, C. J., Chen, D., Yao, Z., and Lei, Y.: NO_x emission trends for China, 1995–2004: The view from the ground and the view from space, J. Geophys. Res., 112, D22306, doi:10.1029/2007JD008684, 2007.

Zhang, X., Friedl, M. A., and Schaaf, C. B.: Global vegetation phenology from Moderate Resolution Imaging Spectroradiometer (MODIS): Evaluation of global patterns and comparison with in situ measurements, J. Geophys. Res., 111, G04017, doi:10.1029/2006JG000217, 2006.

Zhao, C. and Wang, Y. H.: Assimilated inversion of NO_x emissions over east Asia using OMI NO_2 column measurements, Geophys. Res. Lett., 36, L06805, doi:10.1029/2008GL037123, 2009.

Title Page

Abstract | Introduction

Conclusions | References

Tables | Figures

◄ | ►

◄ | ►

Back | Close

Full Screen / Esc

Printer-friendly Version

Interactive Discussion

Table 1. Published estimates of global soil NO_x emissions (S_{NO_x}, $Tg\,N\,yr^{-1}$).

Reference	Fert[1]	N Dep[2]	Above-Soil[3]	Above-Canopy[4]	Description
Galbally and Roy (1978)			10		Average of S_{NO_x} from 3 sites ($3\,ng\,N\,m^2\,s^{-1}$) is multiplied by global land surface area.
Muller (1992)			6.6	4.7	A land-use map is used in combination with the following relationships: (a) Exponential T dependence from Williams et al. (1987)[5] for all soils except tropical forests, (b) Fertilized fields ×3 and (c) Tropical Forests S_{NO_x} ~ 1/precipitation scaled to NPP.
Potter et al. (1996)			9.7		Ecosystem production and soil C-N biosphere model. $S_{NO_x} = f$ (gross mineralized N, WFPS).
Yienger and Levy (1995) (YL95)	1.2		10.2	5.5	Exponential T dependence multiplied by discrete wet/dry biome coefficients; pulsed-N
Davidson and Kingerlee (1997)			21	13	100 measurements (60 refs). Average computed over 17 landtypes and extrapolated globally.
Jaeglé et al. (2005)	2.5–4.5			8.9	Satellite inferred emissions from GOME for the year 2000.
Yan et al. (2005)	1.08[6]		7.4	5.0	A statistical model was developed based on 92 measurements (30 refs) including SOC, pH, landcover, climate, and N-input coupled with exponential T dependence and pulsed-N.
Stehfest and Bouwman (2006)	1.8				A statistical model was developed from 189 (210) NO measurements from 58 (52) refs. over fertilized (natural) soils. Significant variables for fertilized soils: N application/content and climate. Natural soils: biome, SOC, pH, bulk density and drainage.

Title Page

Abstract | Introduction

Conclusions | References

Tables | Figures

Back | Close

Full Screen / Esc

Printer-friendly Version

Interactive Discussion

Table 1. Continued.

Reference	Fert[1]	N Dep[2]	Above-Soil [3]	Above-Canopy[4]	Description
Steinkamp and Lawrence (2011)			10.5/33[7]		Updates YL95 wet/dry biome coefficients using 560 measurements (180 refs). Wet/dry criteria now based on vol. soil moisture. # biomes increased by ×2, fertilizer maps updated.
This study GEOS-Chem Original	0.8 (0.62)[8]		7.4	6.2	YL95 as implemented into GEOS-Chem in Wang et al. (1998)
This study BDSNP (Year 2006)	1.8[8]	0.5	10.7		Updates YL95 including a continuous dependence on soil moisture, modified length/strength of pulsed-N emissions, improved N-fertilizer and manure representation, and the fertilization effect of N-deposition to natural soils.

[1] Estimates of S_{NO_x} resulting from fertilizer and manure-N inputs to soil.

[2] Above canopy estimates of S_{NO_x} resulting from wet and dry-deposited N inputs to soil.

[3] Global above- soil estimates of S_{NO_x}.

[4] Global estimates of S_{NO_x} including canopy uptake of NO_2.

[5] $\log_{10}$ (NO flux) = $0.049 \times T_a - 0.83$, T_a = surface air temperature.

[6] 0.57 Tg N yr^{-1} from chemical fertilizer application and 0.51 Tg N yr^{-1} manure application.

[7] 10.5 (33) Tg N yr^{-1} if using geometric (arithmetic) mean of $A_{w/d}$ calculated over measurements for each landtype.

[8] Above-soil estimate.

Yearly Average Soil NO$_x$ Emissions

(a) YL95 model (original)   **(b) BDSNP (new)**

Global: 7.4 Tg N yr^{-1} Global: 10.7 Tg N yr^{-1}

[ng N m^2 s^{-1}]
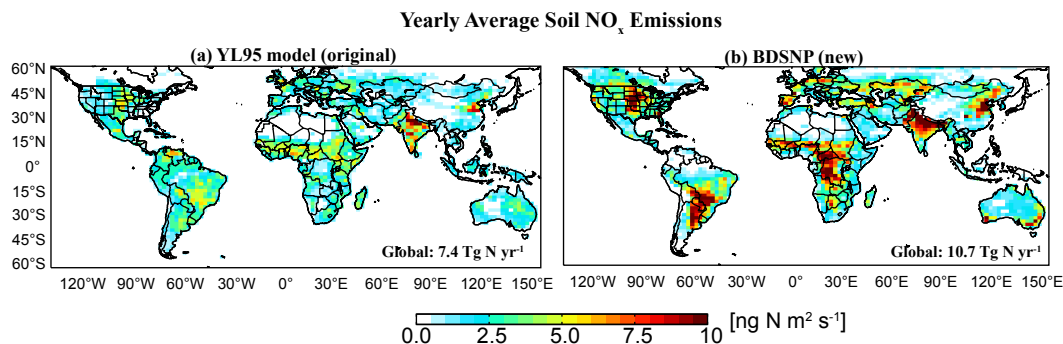
Fig. 1. Comparison of above-soil NO$_x$ emission inventories. Emissions calculated from **(a)** the original YL95 parameterization as implemented into GEOS-Chem (Wang et al., 1998) are compared with **(b)** the updated model (BDSNP) for the year 2006. Calculated global 2006 emissions are listed (lower right). Color bar saturates at 10 ng N m^2 s^{-1}.
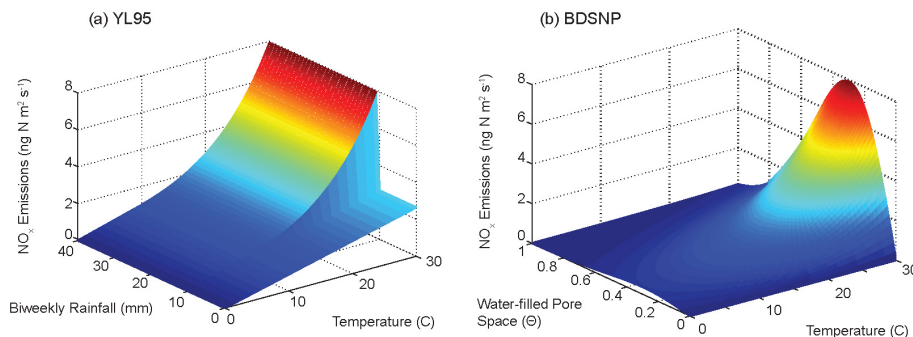
Fig. 2. A three-dimensional representation of the soil NO$_x$ emissions dependence on soil moisture and temperature from **(a)** YL95 and **(b)** BDSNP. The color scheme is a visual aid and follows the vertical axis.
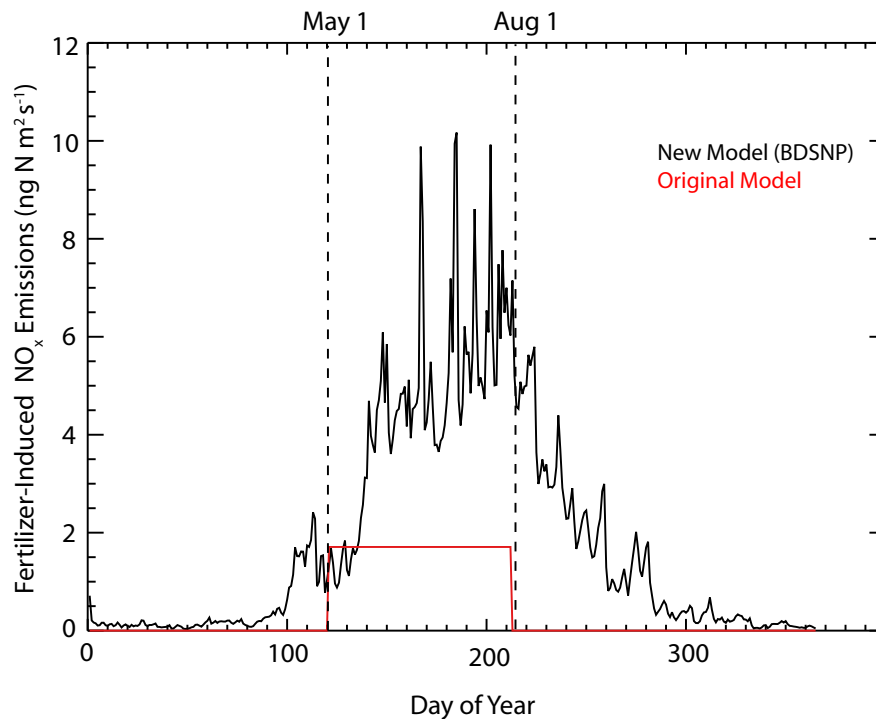
Fig. 3. Mean simulated fertilizer-induced soil NO$_x$ emissions over the central United States (103.75–93.75° W, 27–51° N) for the original GEOS-Chem parameterization (red) and the BD-SNP (black).

Beginning of Growing Season — End of Growing Season

1   92   183   274   365   [day of year]
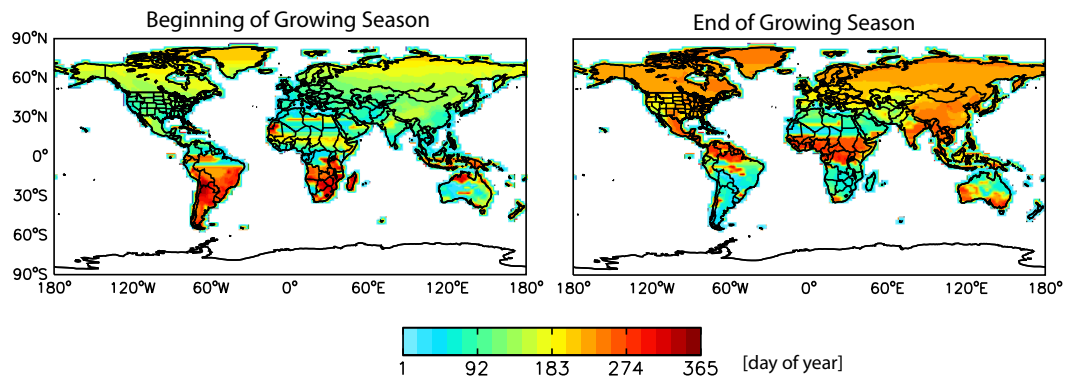
Fig. 4. Beginning and end of the growing season determined using MODIS enhanced vegetation index as described in the text.
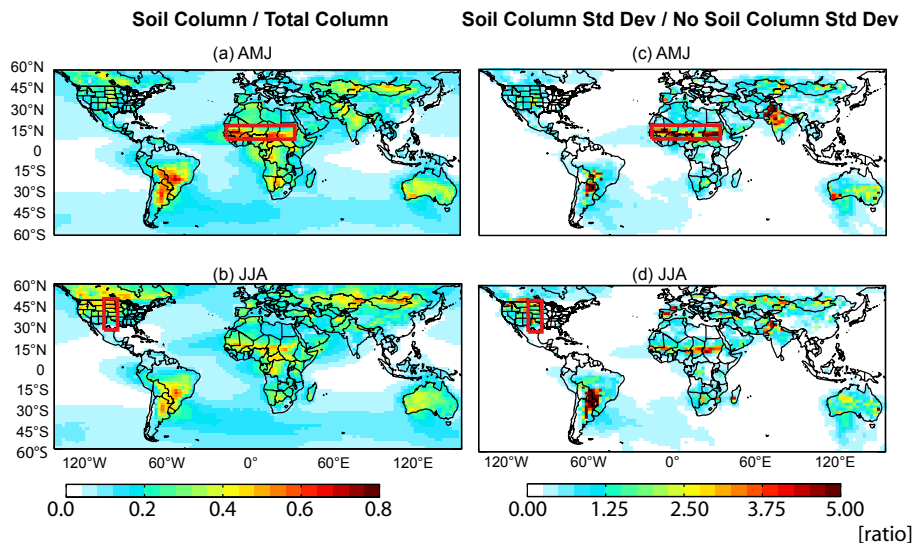
Fig. 5. Sensitivity of simulated tropospheric NO_2 column densities to NO_x emissions from soils for late spring and summer. Shown are **(a, b)** the mean simulated contribution of soil NO_x emissions to the tropospheric NO_2 column and **(c, d)** the ratio of the soil column standard deviation to the simulated tropospheric NO_2 column standard deviation without soil NO_x emissions. The soil column is defined as the difference in the tropospheric NO_2 column between a simulation with and without soil NO_x emission. Boxed regions show the Sahel region of northern equatorial Africa and the Great Plains agricultural center of the United States.
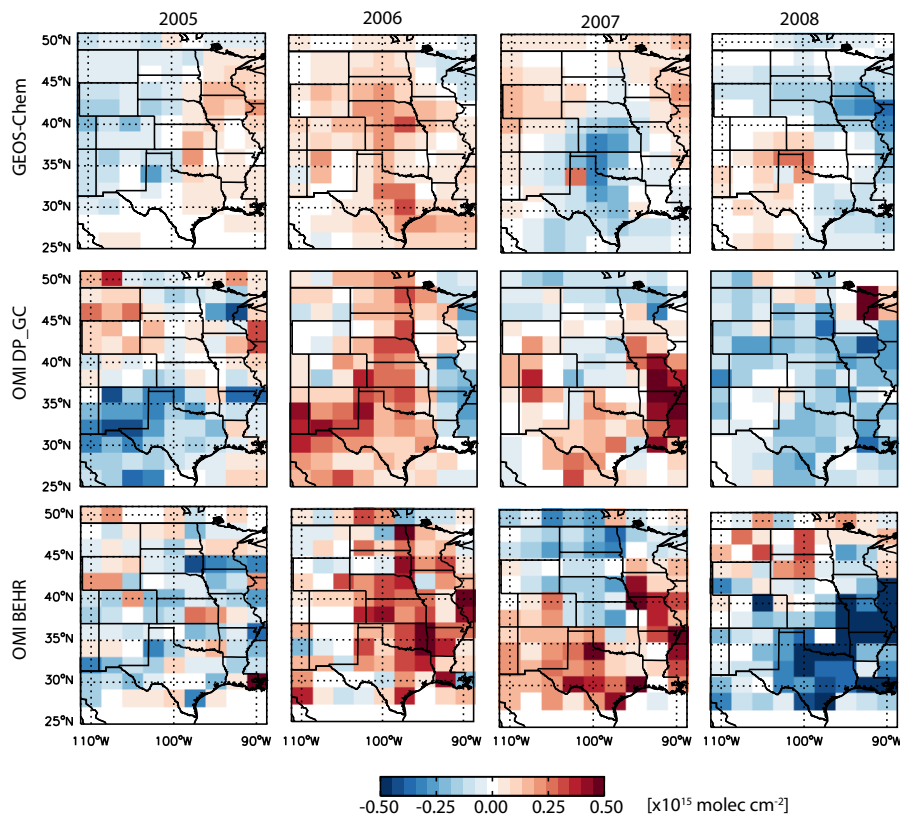
Fig. 6. June mean GEOS-Chem tropospheric NO_2 column density anomalies are compared to mean anomalies for OMI NO_2 from the DP_GC retrieval and the BEHR retrieval. Anomalies are calculated as the difference with the June 2005–2008 mean. Color bar saturates at both ends.
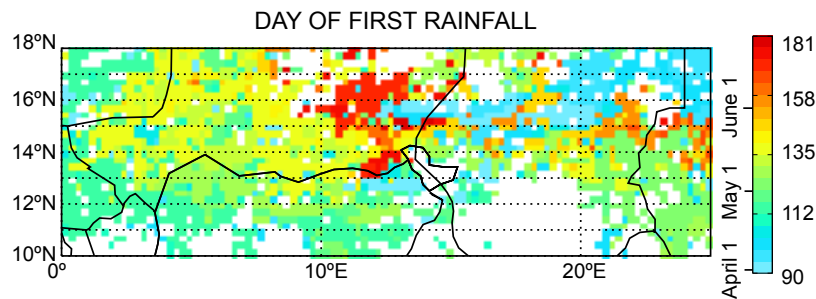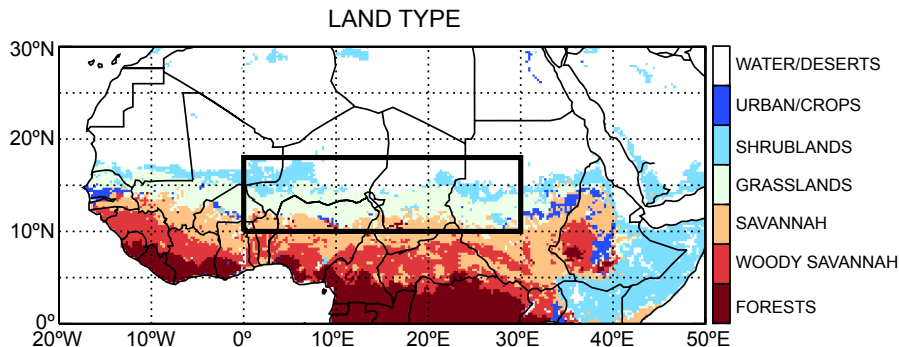
Fig. 7. Land type (top) and first rainfall dates (bottom) over the central Sahel region of northern equatorial Africa (0–30° W, 10–18° N, boxed region). Land types were defined using NASA TERRA/MODIS HDF-EOS MOD12Q1 V004 land cover data. First rain is calculated as the date when TRMM total rainfall exceeds 2 mm in the 24 h period before the OMI overpass time (13:30 UTC–13:30 UTC) following at least 60 days of $<2\,\mathrm{mm\,day^{-1}}$. Regions that do not meet the criteria for dryspell length are shown in white.

OMI VCD enhancements after first rainfall over African Sahel
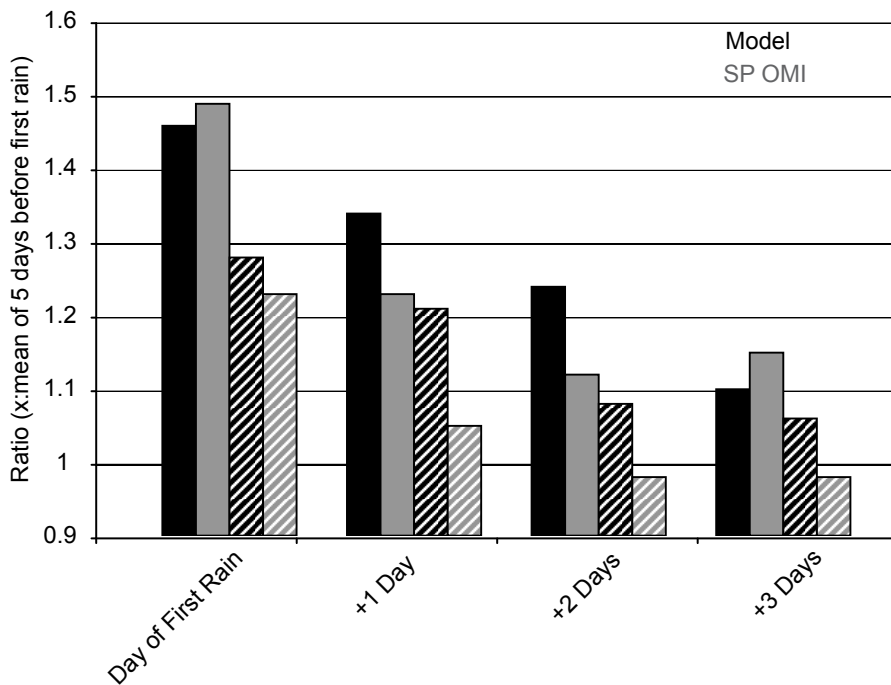
Fig. 8. Mean (solid) and median (diagonal lines) enhancements in the OMI Standard Product (grey) and GEOS-Chem (black) tropospheric NO_2 vertical column densities (VCDs) following the first rainfall of the wet season (April-June 2006) over the African Sahel grasslands (0–30° W, 10–18° N, boxed region in Fig. 7a) are shown. Ratios are taken against the average VCD in the 5 days preceding the first rainfall. All OMI VCD data are averaged daily to 0.25° × 0.25° latitude/longitude resolution where cloud radiance fraction <50 %.

Title Page

Abstract | Introduction

Conclusions | References

Tables | Figures

◀◀ | ▶▶

◀ | ▶

Back | Close

Full Screen / Esc

Printer-friendly Version

Interactive Discussion